Appl Magn Reson (2012) 42:577–584
DOI 10.1007/s00723-012-0332-y

Applied
Magnetic Resonance

Structural Features of Amorphous Silica from Plants

L. A. Zemnukhova · T. A. Babushkina · T. P. Klimova · A. M. Ziatdinov · A. N. Kholomeiydik

Received: 3 October 2011 / Revised: 21 March 2012 / Published online: 24 April 2012

Abstract The data on the structural features of the plant and mineral silica studied by infrared spectroscopy, electron spin resonance and nuclear magnetic resonance ^{1}H porometry methods are compared with analytical and the X-ray phase analysis data. It was shown that the structural features depend on the precursor raw material and on the silica extraction technique. However, the structure of silica obtained from plants principally is not different from that of silica of mineral origin. The pore size on plant silica is smaller than that on mineral silica.

1 Introduction

A step in the evolution of life on the Earth is the emergence of siliciphilous plants. The rice and oats' fruit shells obtained as remainders at the groat-factories contain about 4–20 % amorphous silica. The cheapness and sustainability of that raw plant material is attractive to investigators [1]. Earlier [2–4], we studied the properties of amorphous silica from siliciphilous plants and the mineral remainders [5]. We revealed a correlation between the silica structure and the procedure for silica extraction from the raw material. The main goal of the study was to compare the structural features of amorphous silica from raw plant materials (*Equisetum gen.*, larch and fir trees, seaweeds), cultural plants (rice and oats), and silica of mineral origin.

L. A. Zemnukhova · A. M. Ziatdinov · A. N. Kholomeiydik
Institute of Chemistry, Far Eastern Branch, Russian Academy of Sciences, Vladivostok, Russian Federation

T. A. Babushkina (✉) · T. P. Klimova
Nesmeyanov Institute of Organoelement Compounds, Russian Academy of Sciences, Vavilov str., 28, 119991 Moscow, Russian Federation
e-mail: tab@ineos.ac.ru

In this work, we systematized the data on the structural features of the plant and mineral silica studied by various chemical and physical methods [6–8].

2 Experimental

The compounds studied, the extraction procedures, X-ray phase analysis (XPA) data, analytical data, and the electron spin resonance (ESR) data are listed in Table 1.

The content of silica in the samples varied from 67 to 99.99 % and the maximum content of water was 15 %. Burning of amorphous silica at 1,273 K for 1 h resulted in different crystalline forms (tridymite, crystobalite, quartz, etc.) or did not change the amorphous state depending on the impurity of cations and on the sample origin. After this procedure, the specific surface area (S_{sp}) of the samples decreased from 300 to 8 $m^2\ g^{-1}$.

Infrared (IR) spectra of the samples of amorphous silica and its crystalline forms were obtained on a Shimadzu spectrometer in the range 400–4,000 cm^{-1} in Nujol mulls.

ESR spectra were obtained on an X-band Bruker EMX 6.1 spectrometer (Germany). The modulation amplitude was 0.5 mT and the microwave power was 20 mW. The g factor values of the ESR signals were calibrated against the g factor value of the ESR signal of the conduction electron of metallic Li nanoparticles in a LiF:Li reference sample (the width of the signal is about 0.027 mT and the g factor is 2.002293 ± 0.000003).

The porosity of humid silica samples was investigated by nuclear magnetic resonance (NMR) porometry [9] on a Bruker WM-250 spectrometer (Germany) in the temperature range from 200 to 298 K using deuterated methanol as external standard. To obtain humid samples, the precursor silica samples were placed in hot water (~373 K), kept for 1 h, and then dried in air with paper filters. The pore diameter was estimated from the Gibbs–Thomson equation $\Delta T = K/d$, where ΔT is the melting point difference between bulk water and water in a small pore, d is the pore diameter, and K is the coefficient dependent on the thermodynamic properties of the liquid (for water $K = 58.3°\ nm^{-1}$).

3 Results and Discussion

Fragments of the IR spectra of the characteristic amorphous silica samples are shown in Fig. 1. Curve 1 corresponds to the samples 4 and 11 (see Table 1); curve 2 corresponds to the samples 1, 3, and 5; curve 3 corresponds to anhydrous sample 12, and curve 4 corresponds to sample 15.

The IR spectra of all samples (Fig. 1, curves 1–4) show three bands in the range 460–480, 785–800, and 1,020–1,100 cm^{-1}. They are characteristic of the Si–O–Si siloxane bond. The spectra of samples 4 and 15 (curves 1 and 4) show strong bands at 950 and 920 cm^{-1} originating from the silanol Si–OH bond vibrations. In the IR spectra of curves 2 and 3, these bands are observed as a weak shoulder that points to

Table 1 The silica samples and their characteristics

Sample no.	SiO_2 origin, preparation procedure	XPA data	Content (%)				ESR spectrum
			SiO_2	H_2O	Fe	Mn	
Vegetable raw material							
1	Husk rice (China, treatment HCl → burning [2, 3]	Amorphous	99.2	0.4	0.08	0.03	Yes (Fig. 2, *1*)g_2, g_4
2	The same; after heating to 1,000 °C	Crystal (crystobalite)	99.7	–	0.08	0.03	No Fig. (2, *11*)
3	Husk rice (Far East) → treatment HCl → burning [2, 3]	Amorphous	99.3	0.1	0.13	0.02	Yes (Fig. 2, *1*) g_2, g_4
4	Husk rice (Far East) → treatment NaOH → filter → sedimentation by solution HCl [6]	Amorphous	88.5	11.3	0.04	0.02	No (Fig. 2, *11*)
5	Husk oats → burning [4]	Amorphous	75.7	0.2	0.13	0.12	Yes (Fig. 2, *5*) g_1, g_5Mn
6	Husk oats → treatment HCl → burning [4]	Amorphous	94.3	0.5	0.07	0.02	Yes (Fig. 2, *1*) g_2, g_4
7	Horse-tail forest stems → treatment HCl → burning	Amorphous-crystal (quartz)	88.4	1.6	0.20	0.04	Yes (Fig. 2, *5*) g_5, g_1, g_2
8	Horse-tail wintering stems → burning	Amorphous-crystal (quartz)	67.8	0.6	2.71	0.49	Yes (Fig. 2, *5*) g_5, g_1, g_2
9	Needle of larch from Dauria → burning	Amorphous	83.7	1.7	0.84	0.32	Yes (Fig. 2, *5*) g_1, g_5Mn
10	Needle of larch from Korea → burning	Amorphous-crystal (silicate, oxide and carbonate Ca)	39.6	2.7	0.54	0.96	Yes (Fig. 2, *5*) g_1, g_5 Mn
Technological raw material							
11	$SiO_2 \cdot nH_2O$ (GOST 214-78, Russia)	Amorphous	88.4	11.5	0.04	–	No (Fig. 2, *11*)
12	The same; after heating to 1,000 °C	Amorphous	99.9	–	0.04	–	No (Fig. 2, *11*)
13	Silica for TLC	Amorphous	91.5	8.2	0.03	–	No (Fig. 2, *11*)
14	The same; after heating to 1,000 °C	Amorphous-crystal (crystobalite)	99.7	–			Yes (Fig. 2, *10*) g_1, g_5
15	Diatomite	Amorphous-crystal (tridymite)	67.0	14.0	2.66	<0.01	Yes (Fig. 2, *15*) g_1, g_4, g_3

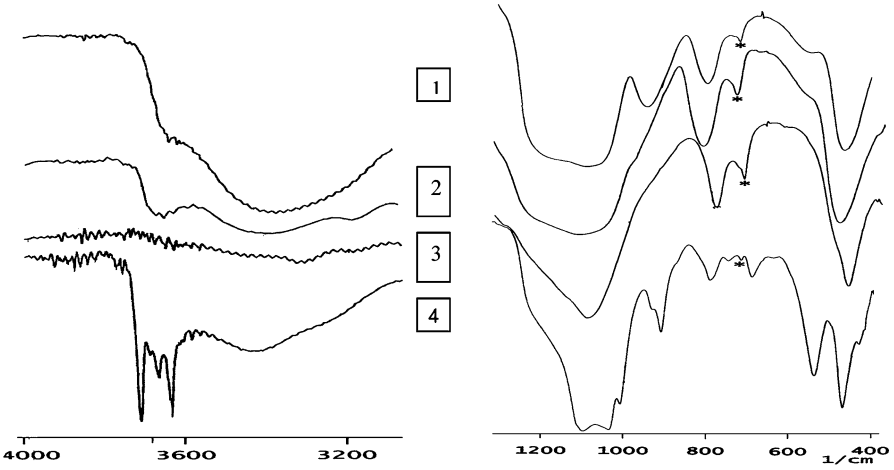

Fig. 1 Fragments of IR spectra of the characteristic samples of amorphous silica *1* samples 4, 11; *2* samples 1, 3, 5; *3* anhydrous SiO_2 (<0.5 %) sample 12; *4* sample 15

a low content of the silanol groups in the samples 1, 3, 5, and 12. This is also confirmed by the absence of absorption in the region of OH-stretching vibrations in the spectrum of anhydrous sample 12 (curve 3). The band at 520 cm^{-1} in the spectrum of sample 15 (curve 4) probably indicates the presence of compounds containing the $(SiO_4)^{4-}$ groups. Narrow lines in the region 3,660–3,600 cm^{-1} in the spectrum of sample 15 may indicate the OH-stretching vibrations in free Si–OH superficial groups or free OH groups of the absorbed water.

Broad bands in the region 3,600–3,660 cm^{-1} in the spectra of curves 1 and 2 correspond to vibrations of free hydroxyl groups of silanol or water in different environment. The absorption bands of hydroxyl groups in water and silanols lie in the region 3,100–3,550 cm^{-1}. The band near 1,220 cm^{-1} in the spectrum of sample 15 suggests that the sample contains compounds with $SiCH_3$ or $SiCH_2$ groups.

Table 1 shows that all silica samples contain metal ions and that their content and oxidation states can vary depending on the treatment procedure (see, e.g., samples 1 and 2; 7 and 8; 13 and 14). Therefore, samples of the same origin can exhibit both ESR signals from paramagnetic ions and ^1H NMR signals from adsorbed water protons. In the presence of paramagnetic ions, these NMR signals should broaden until complete disappearance. The electronic states of these paramagnetic ions were studied by ESR spectroscopy.

The characteristic ESR spectra of the samples studied are shown in Fig. 2. Analysis of the results obtained shows that silicon dioxide samples examined can be divided into several groups according to their ESR spectra.

The first group includes the samples 2, 4, 11, 12, and 13 that produce no ESR signal (Fig. 2, 11), although the atomic absorption analysis data show that all these samples contain iron (from 0.001 to 0.202 %) and manganese (from 0.001 to 0.03 %) (Table 1). Obviously, a simple explanation for the lack of the ESR spectrum of samples 2, 4, 11, 12, and 13 may be a diamagnetic oxidation state of

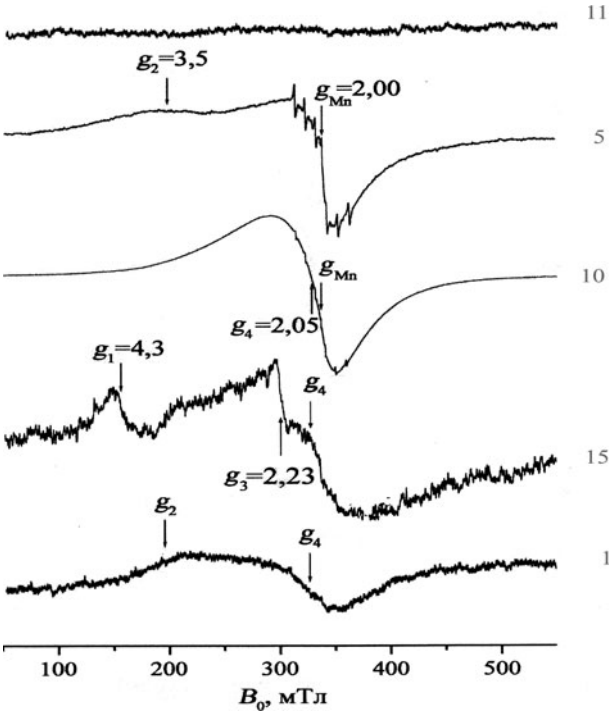

Fig. 2 ESR spectra of amorphous silica samples. The spectra are enumerated according to the sample numbers in Table 1

iron oxide or variation of the crystal field at the paramagnetic ion site, resulting in weak, broad, none uniformly broadened ESR lines. The oxidation state can be changed upon additional heating of the samples (cf. 1–2, 13–14) and upon the change of extraction method it's from the solution (cf. 3–4).

This group includes the samples mainly obtained from mineral (11, 12, 13) and plant (4) raw materials following the same treatment pattern, viz., first, silica was leached in a solution and then precipitated using a hydrochloric acid solution. These uncalcined products contained a large amount of absorbed water (from 3.3 to 11.5 %).

Most samples of both mineral and raw plant origin show complex ESR spectra whose lines are characterized by different g factor values.

The ESR spectra of the samples 5, 7, 8, 9, 10, and 14 comprising group 2 (Fig. 2; 5, 10) are typical of high-spin ions with the $3d^5$ configuration in the crystal field of a weakly distorted tetrahedron or octahedron [10–13]. A characteristic hyperfine structure (HFS) sextet on the broad asymmetric line at $g_5 = g_{Mn} \approx 2.00$ suggests the presence of Mn(ll) ions, which is consistent with the element analysis data (Table 1). The hyperfine constant $A = 8.6$ mT and the spectroscopic splitting factor $g_{Mn} \approx 2.00$ calculated from the magnetic field values are characteristic of Mn ions at oxygen environment [10]. The large width and asymmetry of the line with $g_5 = g_{Mn}$ can be a consequence of the overlap of Mn(ll) HFS lines for four

electronic magnetic transitions at all possible orientations of the powder particles relative to external permanent magnetic field. However, the features of the sample 10 spectrum can also be explained by the overlap of the Mn(ll) line and Fe(lll) ESR line with $g_4 = 2.05$ because the Fe content is 0.38 % (see Table 1).

The ESR spectrum of sample 5 (Fig. 2, 5) shows the resonance line with $g = g_4$ and the sextet HFS characteristic of Mn(II) and also a broad line with $g_2 = 3.5$ characteristic of insulated high-spin states of Fe(lll) and (or) Mn(ll) ions in the octahedral crystal field with a strong rhombohedral or tetrahedral distortion [10–13]. Therefore, in this sample the Fe(lll) and (or) Mn(ll) ions occupy at least two structurally nonequivalent positions of different types.

The ESR spectrum of sample 1 (Fig. 2, 1) shows no sextet HFS characteristic of Mn(ll). In other respects, the spectra of samples 1 and 5 are qualitatively identical.

Note that the spectra of the samples 7 and 8 also exhibit weak broad lines with $g_1 = 4.3$ and $g_2 = 3.5$.

The complex spectrum of sample 15 (diatomite extracted from the raw material formed from seaweed deposits in the course of evolution), exhibits lines with $g_1 = 4.3$, $g_3 = 2.23$, and g_4. According to calculations of ESR spectra of ions with the $3d^5$ configuration [9, 10], the lines with g_1 may correspond to insulated high-spin states of Fe(lll) and (or) Mn(ll) ions in the octahedral crystal field with a strong rhombohedral or tetrahedral distortion. However, the line with g_4 suggests that some impurity ions are in the crystal field with a weakly distorted octahedral or tetrahedral environment [10–13]. The absence of the HFS sextet characteristic of Mn(ll) allows this spectrum to be attributed to mainly Fe(lll) ions. But the signal with $g_3 \approx 2.23$ suggests that some Fe(III) ions forms clusters in which the ions are interconnected by dipole and exchanging interactions [14].

Thus, the ESR data reveal a number of structurally nonequivalent positions of the impurity ions. In particular, Fe and Mn ions can be both in weakly distorted octahedral (or tetrahedral) field environment (g_5 and g_4) and in the environment with a strong rhombohedral or triangular distortion. Treatment of samples by heating to 1,000 °C or the extraction from alkali solution can probably change the oxidation state of Fe ions.

NMR porometry was used to study the "ESR-silent" samples and the silica samples obtained from the horse-tail stems, larch-tree needles, and diatomic seaweeds (humid samples 7, 9, and 15). For comparison, we studied two commercially available silica samples obtained from mineral raw material, namely, "Silica for TLC" (Krasnyj Proletariy, Russia) and "Silicon acid $SiO_2 \cdot n\ H_2O$" (humid samples 11 and 13).

The most surprising is that the ^1H NMR signal of water protons is observed in the humid samples 7, 9, 15 that also exhibit ESR signals. Probably, the pore distribution in the silica matrix and the distribution of paramagnetic ions in its crystal structure are spatially distant from each other. Then, the interaction of spins of water proton in pores with the unpaired electrons of paramagnetic impurity ions can be weak.

The porous structure of a silica sample obtained from husk rice by the two-step oxidative annealing was best studied [6]. The broad (500 Hz) signal of pore water is shifted to weak field (6.6 ppm) compared to the signal of free water (4.8 ppm). Cooling causes an additional down-field shift of the signal, thus indicating a slight

increase in the degree of association of water molecules. It was shown that the pore size depends on the sample treatment procedure. The pore size in the indicated sample was estimated by 8.5 nm, however, in sample 4 it decreased to 1.5 and 4 nm. Correspondingly, the specific surface area obtained from sorption of methylene blue decreased from 309 to 158 $m^2\ g^{-1}$.

The signal of pore water in the sample 7 obtained from horse-tail stems was also shifted to weak field (6.2 ppm) compared to the signal of free water. It was very broad ($\sim$1,000 Hz).The pore size in sample 7 was equal to 3 nm. Apparently, this sample also contained free water that melts at about 272 K.

The signal of sample 9 obtained from larch-tree needles was weaker ad broader than the signal of sample 7. This sample has pores with different size from 1.5 to 2.5 nm.

In the humid sample 6, the ^{1}H NMR signal of water protons was very broad and was not studied by the cooling procedure.

The sample 15 (diatomite) had a small specific surface area of about 80 $m^2\ g^{-1}$. Therefore, it absorbs a small amount of water and its ^{1}H NMR signal of water protons was also weak. In that sample, the water melting point was 271 K. This suggests either a large pore size of nearly 30 nm or the presence of free water between the grains of the sample.

For the mineral silica samples, the pore size also depends on the extraction technique. In particular, "Silicon acid $SiO_2 \cdot n\ H_2O$" has pores of two sizes, namely, 1 and 7 nm, but 'Silica for TLC' has only 7-nm pores.

The melting point of water in the pores depends on the pore size (Fig. 3). The largest range of changes in the melting point of water ($\Delta T = 48°$) was found for

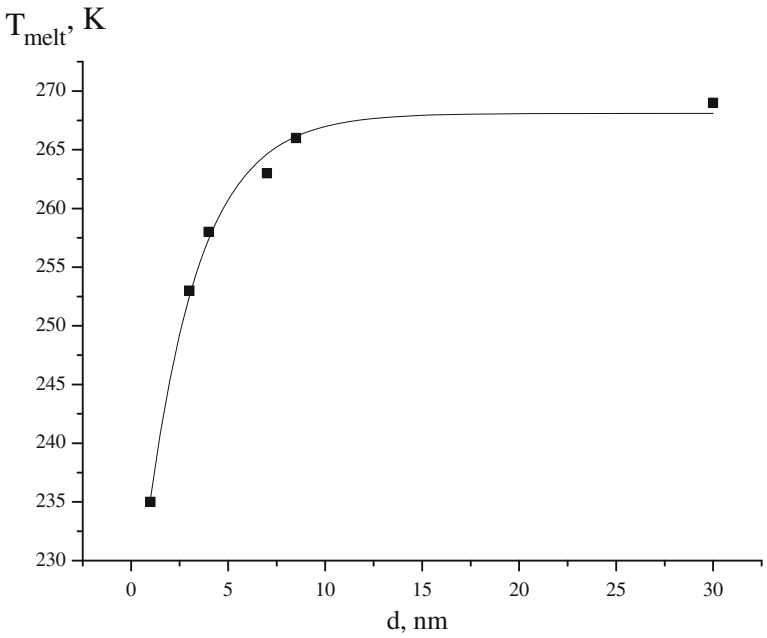

Fig. 3 Melting point of water in pores plotted versus pore sizes from ^{1}H NMR porometry data

small-diameter pores (0.9/4 nm). For larger pores (4/45 nm), the changes occur with in a temperature range of 14°; therefore, the size of large pores is determined with much lower accuracy compared to the small pore size.

Thus, IR and EPR spectroscopy and ^{1}H NMR porometry data suggest that the properties of silica obtained from plants are slightly different from those of silica of mineral origin. Namely, the silica content in all samples is 60–70 %; the specific surface area of amorphous silica samples burnt below 1,000 K exceeds 50 m^2/g; all samples contain Fe^{2+} paramagnetic ions, although in different concentrations. The sorption properties of silica can also be different because they depend on the material porosity. The pore size in plant silica is smaller than in mineral silica. Important advantages of plant silica include the availability of raw material and a nearly constant chemical composition of silica provided the same method of silica extraction from the same raw material.

References

1. V.I. Sergienko, L.A. Zemnukhova, A.G. Egorov, E.D. Shkorina, N.S. Vasilyk, Russ. Chem. J. **48**, 116–124 (2004)
2. L.A. Zemnukhova, G.A. Fedoristcheva, A.G. Egorov, V.I. Sergienko, Russ. J. Appl. Chem. **78**, 324–328 (2005)
3. L.A. Zemnukhova, A.G. Egorov, G.A. Fedoristcheva, N.N. Barinov et al., Russ. J. Inorg. Matirial. **42**, 27–32 (2006)
4. L.A. Zemnukhova, V.V. Budaeva, G.A. Fedoristcheva, T.A. Kaiidalova, L.N. Kurilenko et al., Russ. J. Chem. Plant Raw Material, 147–152 (2009)
5. L.A. Zemnukhova, G.A. Fedoristcheva, E.D. Shkorina, T.A. Kaiidalova, N.N. Barinov, Russ. J. Appl. Chem. **84**, 529–535 (2011)
6. L.A. Zemnukhova, T.A. Babushkina, T.P. Klimova, Russ. J. Gen. Chem. **77**, 917–922 (2007)
7. L.A. Zemnukhova, T.A. Babushkina, T.P. Klimova, A.N. Kholomeiydik, Russ. J. Appl. Chem. **83**, 203–206 (2010)
8. L.A. Zemnukhova, Yu.M. Nikolenko, Russ. J. Gen. Chem. **81**, 602–608 (2011)
9. O.V. Petrov, I. Furo, Progr. NMR Spectrosc. **54**, 97–122 (2009)
10. R.C. Nicklin, H.A. Farach, C.P. Poole, J. Chem. Phys. **65**, 2998–3005 (1976)
11. Fu-Cheng Lin, Scientia Sinica A **25**, 1298–1304 (1982)
12. M. Toderas, I. Ardelean, J. Optoelectron. Adv. Mater. **9**, 629–632 (2007)
13. I. Ardelean, C. Andronache, C. Cimpean, P. Pascuta, J. Optoelectron Adv. Mater. **8**, 1372–1376 (2006)
14. V.F. Anufrienko, L.G. Yandralova, D.V. Tarasova, Russ. Phys. Solid State **13**, 2353–2356 (1971)